PERGAMON

Journal of Structural Geology 25 (2003) 1359–1370

JOURNAL OF STRUCTURAL GEOLOGY

www.elsevier.com/locate/jsg

Deformation of ductile inclusions in a multiple inclusion system in pure shear

Nibir Mandal[a], Susanta Kumar Samanta[a], Gautam Bhattacharyya[a], Chandan Chakraborty[b,*]

[a]*Department of Geological Sciences, Jadavpur University, Calcutta 700032, India*
[b]*Geological Studies Unit, Indian Statistical Institute, 203, B.T. Road, Calcutta 700035, India*

Received 22 April 2002; received in revised form 26 November 2002; accepted 6 December 2002

Abstract

This paper analyzes the deformational behavior of mutually interacting spherical inclusions in a multiple inclusion system, considering two physical factors: viscosity ratio between inclusion and matrix (m) and the ratio of inclusion diameter to mean inter-inclusion distance (a/b). For a given value of m, the strain partitioning between a stiff inclusion and the bulk system (i.e. ratio of their natural extension rates) increases non-linearly with increasing a/b ratios and the gradient of increase becomes steeper when the inter-inclusion distance is less than about twice their diameter (i.e. $a/b >$ about 0.5). The strain distribution within a deformed inclusion is homogeneous when the a/b ratio is less than about 0.6. For larger values of a/b, the internal deformation becomes heterogeneous, with the strain increasing or decreasing towards the core in the case of stiff ($m > 1$) and soft ($m < 1$) inclusions, respectively. The deformed shape of inclusions in section also shows departure from an ideal ellipse with an increase in the a/b ratio. Stiff inclusions develop shapes similar to that of a super-ellipse in contrast to soft inclusions that resemble a sub-ellipse. The heterogeneity of internal deformation is also reflected in the distortion of passive foliations initially at right angles to the bulk extension direction, which become curved with convexity outward and inward, respectively, within stiff and soft inclusions.

Keywords: Inclusion; Viscosity contrast; Heterogeneous strain; Matrix; Flow field

1. Introduction

Deformed objects, e.g. pebbles, ooids, are widely used in the estimation of geological strain of rocks (Ramsay, 1967; Gay, 1968b; Gay and Fripp, 1976; Lisle et al., 1983; Ramsay and Huber, 1983; Lisle, 1985; Freeman, 1987; Ramsay and Lisle, 2000). To be able to determine strain, we need to know how an inclusion deforms depending upon its initial shape and its competence contrast with the matrix. According to theoretical results, *isolated* inclusions of ellipsoidal initial shape deform homogeneously, and the axial ratios of their flattened shapes depend on the ratio of inclusion and matrix viscosities, in addition to the bulk strain (Eshelby, 1957; Gay, 1968a; Bilby et al., 1975). In a recent study Treagus and Treagus (2001) have shown that the finite strain of ellipsoidal inclusions depends also on their initial axial ratios. For a given finite bulk strain, competent inclusions with axial ratios of three or more undergo more strain than equant inclusions of the same viscosity, whereas the reverse is true when the inclusions are incompetent. The deformational behavior of inclusions with non-ellipsoidal initial shapes is much more complex (Treagus et al., 1996; Treagus and Lan, 2000; Treagus, 2002). The strain in them is heterogeneous, and their deformed shapes are remarkably different from those that would have been developed by an overall homogeneous strain.

All the studies discussed above deal with *isolated* inclusions. In this paper we study the deformational behavior of mechanically interacting spherical inclusions in a multiple inclusion system undergoing pure shear. With the help of Lamb's (1932) theory we derive the velocity functions for flow inside and outside an inclusion in their interacting state (Happel, 1957), and analyze the strain partitioning between a stiff inclusion and the matrix. The results are used in two-dimensional numerical models to show how the concentration of inclusions affects strain

* Corresponding author. Fax.: +91-33-577-6680.
E-mail address: chandan@isical.ac.in (C. Chakraborty).

0191-8141/03/$ - see front matter © 2003 Elsevier Science Ltd. All rights reserved.
doi:10.1016/S0191-8141(02)00204-3

partitioning, deformed, inclusion shape, and the strain distribution and distortion patterns of passive foliations in both stiff and soft inclusions. The numerical simulations are compared with results of laboratory experiments.

2. Theoretical model

We consider a system of deformable, spherical inclusions of diameter $2a$ within a Newtonian viscous matrix with coherent interfaces (Fig. 1). The inclusions are uniformly distributed with their centers spaced at an interval of $2b$. The system is subjected to pure shear deformation at a rate $\dot{\epsilon}$. To describe the flow field around an inclusion a Cartesian coordinate frame is chosen at the center of an inclusion with the x axis parallel to the bulk extension direction, y axis along the direction of principal shortening, and z axis along the direction of no bulk flow (Fig. 1). We adopt Lamb's (1932) method of analysis that expresses the velocity field in terms of solid harmonic functions, and derive the velocity functions in three dimensions for flow inside and outside an inclusion in a multiple inclusion system (details given in Appendix A). In the numerical analysis, for convenience, we consider the velocity functions on a two-dimensional section perpendicular to the direction of no bulk strain. The section is chosen at $z = 0$. The following analysis deals with the circular cross-section of the inclusion on that plane. The velocity functions (Eqs. (A5) and (A6a)–(A6c)) on the $z = 0$ plane are as follows.

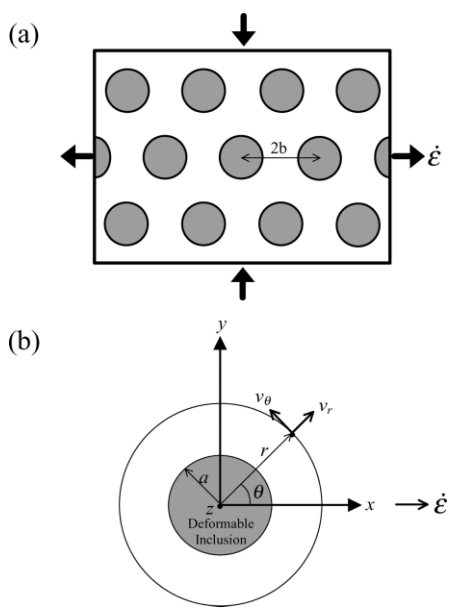

Fig. 1. (a) Model of the inclusion–matrix system under theoretical considerations. (b) Consideration of Cartesian and spherical coordinates on the central section of an inclusion normal to the direction of no bulk flow (z axis). $\dot{\epsilon}$: pure shear rate of bulk deformation. $2a$: diameter of inclusions (shaded) and $2b$: average inter-inclusion distance.

Velocity components of flow outside the inclusion:

$$u = \frac{C_2}{21}\frac{r^2}{a^2}\left(5 - 2\frac{x^2 - y^2}{r^2}\right)x + \frac{1}{2}A_{-3}\frac{a^3}{r^3}\frac{x^2 - y^2}{r^2}x + B_{-3}\frac{a^5}{r^5}\left(2 - 5\frac{x^2 - y^2}{r^2}\right)x + \frac{1}{2}Kx + \dot{\epsilon}x, \tag{1a}$$

$$v = \frac{C_2}{21}\frac{r^2}{a^2}\left(-5 - 2\frac{x^2 - y^2}{r^2}\right)y + \frac{1}{2}A_{-3}\frac{a^3}{r^3}\frac{x^2 - y^2}{r^2}y + B_{-3}\frac{a^5}{r^5}\left(-2 - 5\frac{x^2 - y^2}{r^2}\right)y - \frac{1}{2}Ky - \dot{\epsilon}y. \tag{1b}$$

Velocity components of flow inside the inclusion:

$$u' = \frac{A_2}{21}\frac{r^2}{a^2}\left(5 - 2\frac{x^2 - y^2}{r^2}\right)x + 2B_2x, \tag{2a}$$

$$v' = \frac{A_2}{21}\frac{r^2}{a^2}\left(-5 - 2\frac{x^2 - y^2}{r^2}\right)y - 2B_2y, \tag{2b}$$

where $r^2 = x^2 + y^2$ and a is the radius of inclusion. K, C_2, A_{-3}, B_{-3}, A_2, B_2 are constants, the expressions for which involve the ratio of inclusion diameter and mean inter-inclusion distance (a/b) and the viscosity ratio between inclusion and matrix (m) (Eq. (A19) of Appendix A). The velocity functions in Eqs. (2a) and (2b) reflect the nature of deformation of an inclusion in inclusion-matrix systems. In these equations, A_2 becomes nearly zero when the a/b ratio is extremely low, indicating a homogeneous deformation inside the inclusion as in the case of a single inclusion system (cf. Eshelby, 1957; Gay, 1968a). But, A_2 becomes a non-zero quantity for higher values of a/b, implying that the deformation is heterogeneous when the inclusions are closer to one another in the system.

We analyzed deformation of an inclusion in two dimensions using the velocity functions (Eqs. (2a) and (2b)) by varying the viscosity ratio between inclusion and matrix (m) and the a/b ratio, which is considered a measure of concentration of inclusions in the inclusion-matrix system. The results are presented in the following sections.

3. Deformation of ductile inclusions

3.1. Strain partitioning between stiff inclusions and the bulk rock

This analysis can be applied to understand the control of inclusion concentration in a multiple-inclusion system (i.e. a/b ratio) on strain partitioning between matrix and inclusion. Differentiating Eq. (A8a) with respect to r and substituting $r = a$ and $\theta = 0$ in the derived equation, we

obtain:

$$\frac{\dot{\epsilon}_i}{\dot{\epsilon}} = \left[1 - \frac{m-1}{P}\left\{\left(\frac{a}{b}\right)^3 - \frac{3}{2}Q\frac{\left(1-\frac{b^7}{a^7}\right)}{19(m-1)+\frac{5}{2}\frac{b^7}{a^7}Q} - 1\right\}\right], \quad (3)$$

where

$$P = \frac{1}{4}\left[\frac{16Q(m-1) - \frac{b^7}{a^7}Q^2}{19(m-1)+\frac{5}{2}\frac{b^7}{a^7}Q}\right] + (m-1)\left(\frac{3}{2}+\frac{a^3}{b^3}\right) + \frac{5}{2}$$

and

$$Q = (19m + 16).$$

$\dot{\epsilon}_i$ is the natural rate of stretching of the inclusion diameter along the bulk extension direction.

Eq. (3) shows that the strain-rate partitioning between a stiff inclusion and the bulk medium, i.e. $\dot{\epsilon}_i/\dot{\epsilon}$, increases non-linearly with the *a/b* ratio, and the non-linear variations depend on the viscosity contrast (*m*) (Fig. 2). For any *m,* the variation of strain partitioning factor ($\dot{\epsilon}_i/\dot{\epsilon}$) with *a/b* is not significant when *a/b* is low, but it becomes significant at a higher *a/b*, the value of which increases with increasing *m*. Again, the rate of change of the strain partitioning factor with *a/b* at high *a/b* is much greater at higher *m* than at lower *m* (Fig. 2). The mathematical calculations reveal that the effect of mechanical interaction on the strain partitioning can be significant when the inter-inclusion distance is low, generally less than about twice their diameter (cf. Shimammoto, 1975, see discussion in Treagus et al., 1996; Treagus and Treagus, 2001).

In order to compare the effect of inter-inclusion distance on the strain partitioning with that of viscosity contrast, we consider a system with inclusions at a very low volume concentration (*a/b* < 0.05). In this case, the ratio of strain rates of inclusion and bulk system increases from 0.04 to 0.4 as the viscosity ratio (*m*) decreases from 40 to 5. On the other hand, for *m* = 40, the strain ratio increases to nearly 0.8 as the *a/b* ratio is increased up to 0.9. This implies that the concentration of inclusions influences the strain partitioning relatively more than the viscosity contrast.

3.2. Shapes of deformed inclusions

Using Eqs. (2a) and (2b) and a simple computer program on Visual Basic we performed numerical simulations to study the nature of shape changes during deformation of an inclusion in an interacting system. These reveal that the deformed shapes of inclusions stiffer than the matrix (*m* > 1) show elliptical geometry at low values of *a/b* ratio (<0.5), as in the case of isolated inclusions (Gay, 1968a). With increase in inclusion concentration, the deformed shapes depart from an ideal ellipse, and tend to assume the geometry of a super-ellipse (Fig. 3; cf. Lisle, 1988). Again, for a given *a/b* ratio the departure of the deformed shapes from elliptical geometry becomes more pronounced with increasing viscosity contrast (*m*) (Fig. 3).

In contrast to stiff inclusions, inclusions softer than the matrix (*m* < 1) develop deformed shapes resembling a sub-ellipse for large values of *a/b* (Fig. 4), as noticed in naturally deformed inclusions (fig. 7.3, Ramsay and Huber, 1983; fig. 39.20, Ramsay and Lisle, 2000). Such non-ideal geometry is more obvious with a decrease in viscosity ratio *m* (Fig. 4). However, for low concentrations of inclusions (*a/b* < 0.5) the deformed shapes show little departure from an ideal elliptical geometry with changing viscosity ratio *m*.

In summary, circular cross-sections of inclusions in an interacting state generally deform into non-ideal elliptical shapes. The deformed shapes of stiff (*m* > 1) inclusions superscribe an ideal ellipse (cf. super-ellipse), whereas those of soft (*m* < 1) inclusions inscribe an ideal ellipse

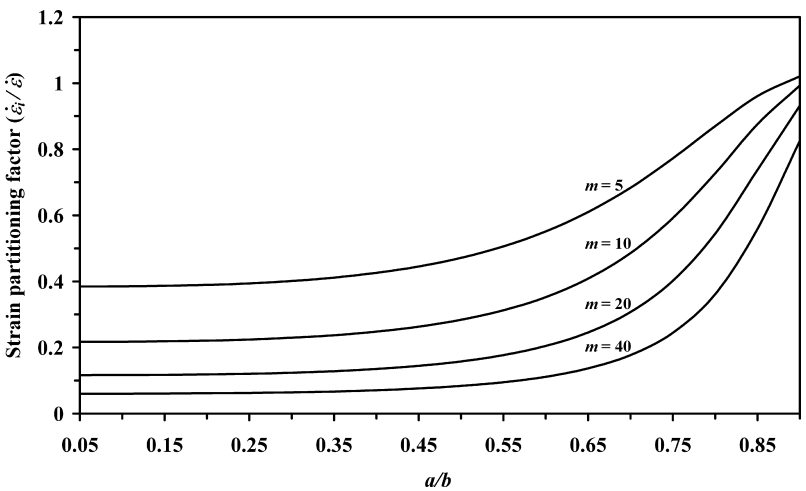

Fig. 2. Calculated plots of the ratio of natural extension rates of stiff inclusions to that of the bulk system as a function of *a/b* ratios for different viscosity ratios *m*.

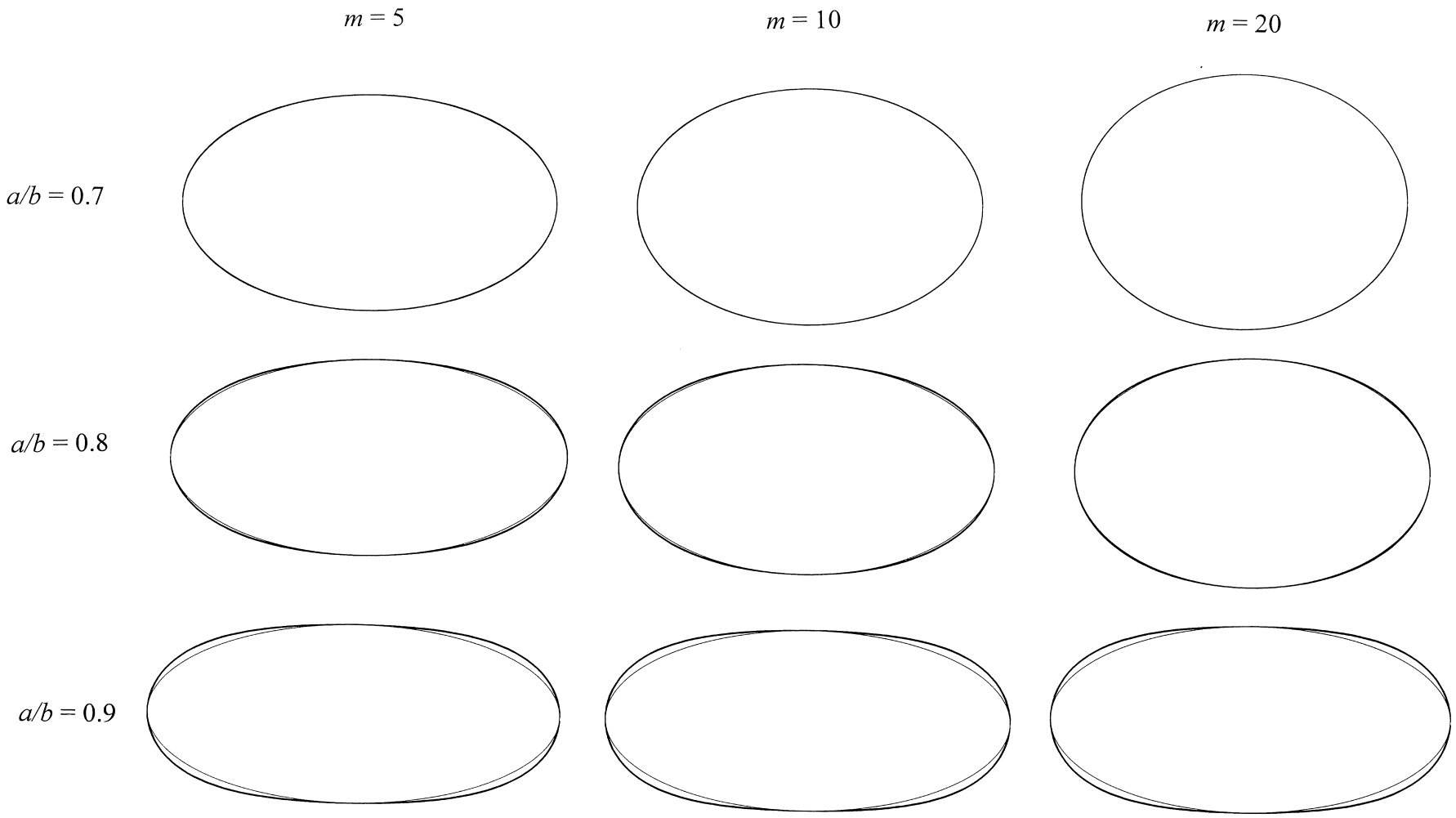

Fig. 3. Deformed shapes of stiff ($m > 1$) circular inclusions in numerical models. *a*/*b*: ratio of inclusion diameter to inter-inclusion distance; *m*: viscosity ratio between inclusion and matrix. Thin solid lines show the shape of corresponding ideal ellipses. Finite strain of models = 0.4.

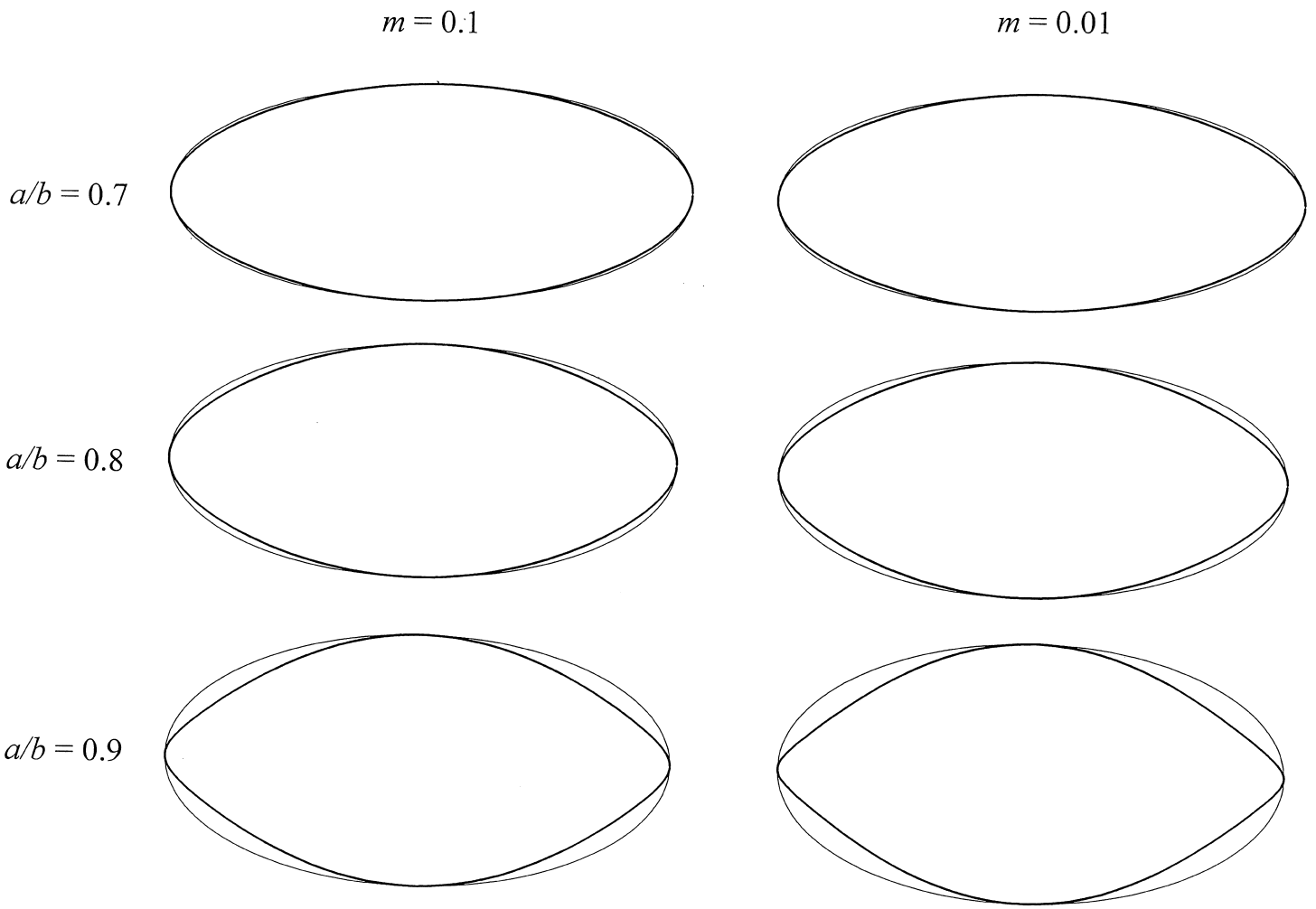

Fig. 4. Deformed shapes of soft ($m < 1$) inclusions in numerical models. Thin solid lines show the shape of the corresponding ideal ellipse. Finite strain of models = 0.4.

(cf. sub-ellipse). Inclusions occurring in low concentrations ($a/b < 0.5$) deform into ideal elliptical shapes, irrespective of the viscosity contrast between the inclusion and matrix.

3.3. Strain distribution inside deformed inclusions

Using the numerical models, we studied the pattern of strain distribution in an inclusion containing circular strain markers, arranged in a Cartesian grid inside the inclusion. A set of experiments was run on models with stiff inclusions ($m > 1$) under varying a/b ratios, keeping the viscosity contrast constant. The strain distribution is virtually homogeneous when $a/b < 0.5$, but shows discernible heterogeneity at larger values of a/b, showing increasing finite strain towards the core of the inclusion compared with the periphery (Fig. 5a).

The nature of strain heterogeneity in inclusions with $m < 1$ is strikingly different from that in inclusions with $m > 1$. In this case the finite strain increases from the center to the periphery of the inclusion. At a large value of a/b ratio ($= 0.9$) the deformed inclusions show localization of high finite strain at the tapered ends of the flattened inclusion, and relatively low strain at the center of the inclusion (Fig. 5b).

3.4. Distortion patterns of passive markers inside inclusions

The heterogeneous deformation of inclusions is reflected in the distortion pattern of internal passive foliations initially perpendicular to the bulk extension direction. Within stiff inclusions ($m > 1$), the markers remain straight when the viscosity ratio is low and the concentration of inclusions is not large ($a/b < 0.5$). In other conditions, the deformed markers become curved, with the convex side facing the bulk extension direction (Fig. 6a). When the inclusions are softer than the matrix (i.e. $m < 1$), passive markers also develop curved shapes. But, the sense of curvature is opposite to that within stiff inclusions (Fig. 6b).

4. Test model verification of the theoretical results

Experiments were conducted on physical models containing a number of deformable inclusions hosted in a viscous matrix of putty. The inclusions were either stiffer or softer than the matrix. Commercial plasticine was used to simulate stiff inclusions and the viscosity ratio of plasticine and putty was estimated to be about four. We prepared soft inclusions with a mixture of wheel-bearing grease and talc powder in a 1:1 volume ratio, which gave a viscosity ratio of

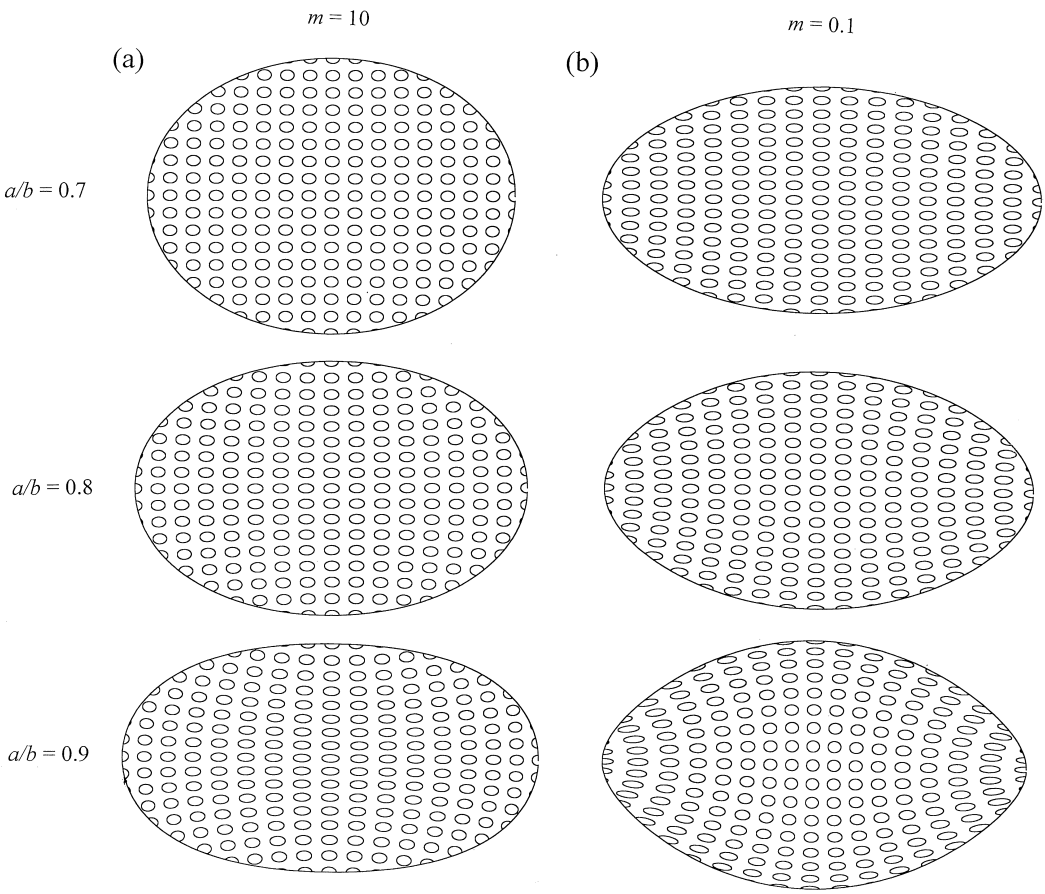

Fig. 5. Heterogeneous strain distributions inside (a) stiff ($m > 1$) and (b) soft ($m < 1$) inclusions in numerical models. Finite strain of models = 0.3.

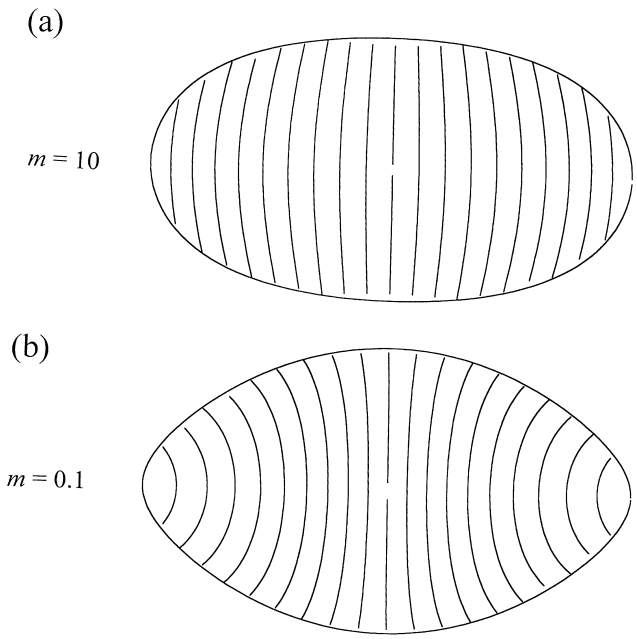

Fig. 6. Distortion patterns of internal markers at right angles to the bulk extension direction within (a) stiff and (b) soft inclusions. $a/b = 0.9$. Finite strain of models = 0.3.

inclusion to matrix of about 0.2. Test models were prepared in the following way. A number of circular, platy inclusions were embedded in a rectangular slab of putty (Fig. 7), with their circular sections exposed to the surface of the model.

Experiments reveal the effect of mechanical interaction on the degree of flattening of the inclusions. The initial model had an inclusion surrounded by a number of closely spaced neighbors. A similar inclusion was kept at a large distance from them to obtain the finite strain of inclusions in a non-interacting state and to compare it with those in the multiple association. It was observed that the central inclusion in the multiple association underwent flattening larger than the far-field inclusion (Fig. 8a). The observation agrees with the theoretical inference that the stretching rate of an inclusion is larger for smaller inter-inclusion distance (Fig. 2). For example, the axial ratio of the deformed far-field inclusion was 1.1, whereas the axial ratio of the central inclusion was 1.3, for a bulk strain ellipse with axial ratio of 2.25. Experimental results thus indicate that in addition to the viscosity contrast (Gay, 1968a; Lisle et al., 1983; Treagus et al., 1996), the concentration of inclusions in the system is another crucial parameter controlling the magnitude of flattening of stiff inclusions.

Model experiments also confirmed the theoretical result that the circular cross-section of an inclusion in an interacting state deforms into a shape departing from that of an ellipse. It was observed that the deformed shape of a stiff inclusion in multiple inclusion system was like a super-ellipse, whereas that of a soft inclusion was like a sub-ellipse (Fig. 8b and c).

Similar experiments on inclusions containing circular or line markers show that the deformation inside inclusions in an interacting state is heterogeneous (Fig. 9a), as obtained in the numerical models (Fig. 5a). Within stiff inclusions, the axial ratio of strain ellipses increases inward, defining a zone of high finite strain in the central part of the inclusion. The heterogeneous deformation also led to curved distortion patterns of passive foliation markers within the inclusions (Fig. 9b), which conforms to those obtained from numerical simulations (Fig. 6a). The deformation inside inclusions softer than the matrix is also heterogeneous, which is reflected in the inwardly convex distortion patterns of markers initially at right angles to the bulk extension direction (Fig. 9c), as in the numerical simulations (Fig. 6b).

5. Discussion

The deformed shapes of inclusions are often used for estimation of bulk strain. In order to do this, we need to consider the strain partitioning between the inclusion and bulk system. Earlier theoretical results show that this depends mainly on the viscosity contrast between inclusion and matrix (Gay, 1968a; Bilby et al., 1975). Our analysis suggests that, for the same viscosity contrast, variations in concentration of inclusions can result in a significant change in the ratio of strain rates of inclusion and the bulk rock. It thus appears that in the use of deformed inclusions for strain analysis their volume concentration needs to be taken into account if they occur in large concentration. It may be noted

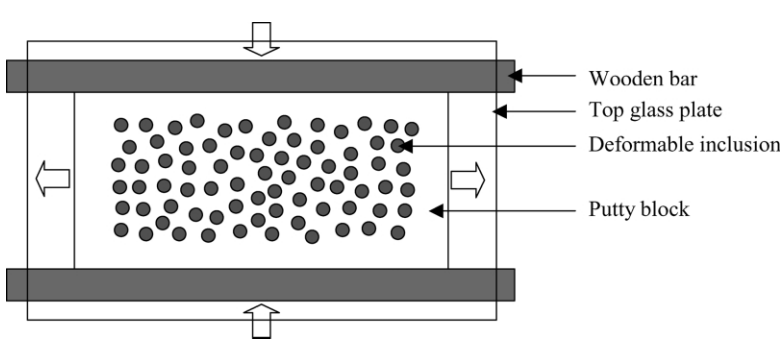

Fig. 7. Schematic sketch of the experimental setup for deformation of models containing ductile inclusions (shaded) embedded in a putty block. The model was deformed under approximate pure shear by moving two vertical rigid bars towards each other (arrows). The flow of the model took place in the horizontal directions, and was restricted in the vertical direction by a horizontal glass plate at the top.

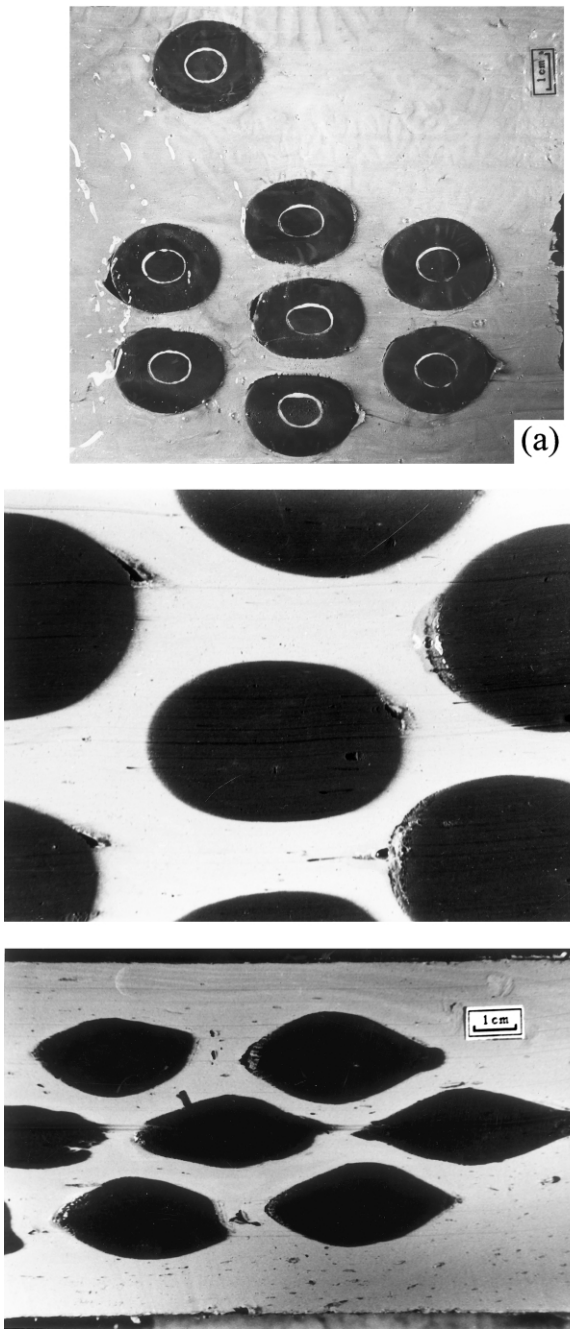

Fig. 8. (a) Contrasting flattening of inclusions occurring in multiple association and that away from them under the same bulk deformation. Note that the isolated inclusion has flattened less than the central one occurring in multiple inclusions. Deformed shapes of inclusions (b) stiffer ($m \approx 4$) and (c) softer ($m \approx 0.2$) than the matrix in test models. The inclusions in the models were initially circular in cross-section, and had more or less similar relative dispositions with $a/b \approx 0.7$. Length of the photo-plate (b) is 3.8 cm.

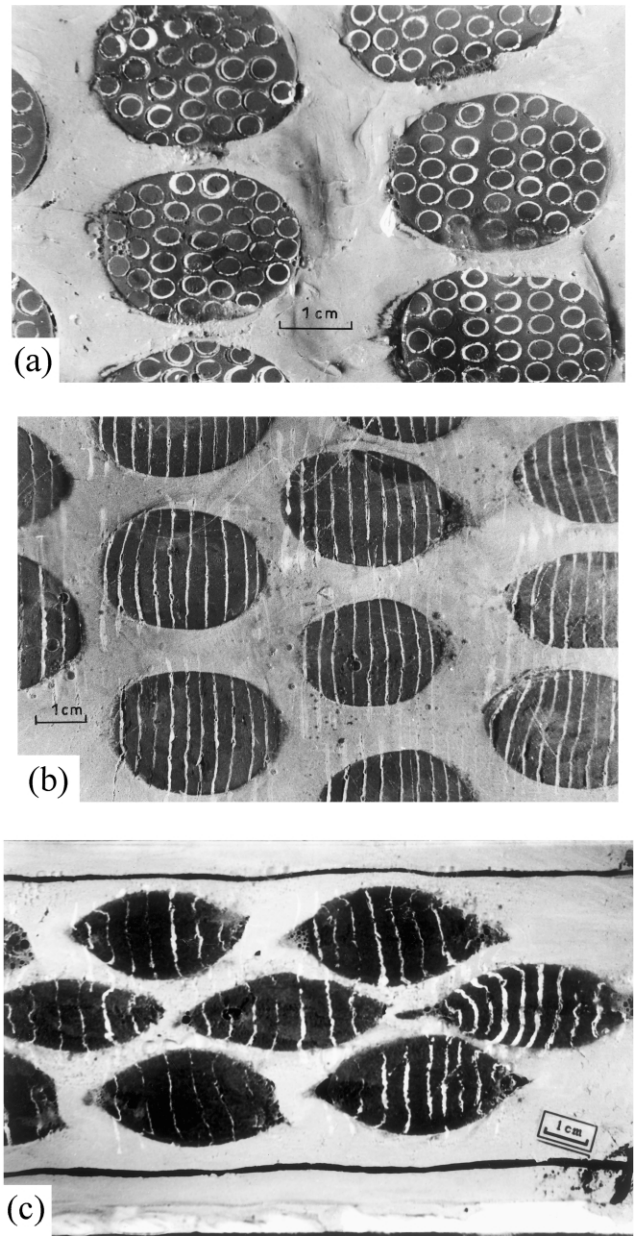

Fig. 9. (a) Heterogeneous strain distributions inside deformed stiff inclusions in test models. Note that the finite strain decreases radially away from the center of inclusions. (b) Deformed models showing outward-convex distortion patterns of passive markers, initially perpendicular to the bulk extension direction within flattened inclusions. (c) Heterogeneous deformation of inclusions softer than the matrix, as reflected from curved distortion patterns of internal passive markers, initially at right angles to the bulk extension direction.

that the strain-partitioning ratio in this analysis has been derived considering a spherical initial shape of the inclusion, although for a given viscosity contrast the strain of stiff inclusions increases with increasing initial axial ratio of elliptical inclusions (Treagus and Treagus, 2001). It thus seems that the ratio of strain rates between inclusion and bulk rock may not remain constant, but is likely to increase as the shape of inclusion departs more and more from a sphere with progressive deformation (Smith, 1975).

Analytical solutions for the flow inside an inclusion show that the deformation within interacting inclusions is heterogeneous, which we also demonstrated in two-dimensional numerical models (*ZX* plane of bulk strain), representing the central section at right angles to the direction of no bulk strain. The same solutions can be

utilized to study the nature of heterogeneous deformation on any section parallel to the *XY* and *YZ* planes of bulk finite strain. We compare the results obtained from these two-dimensional simulations with that observed in physical model experiments, assuming that a thin circular inclusion might be a representative of the central section across a spherical inclusion at a right angle to the direction of no bulk strain. However, the deformation patterns on any other section are likely to be different from those observed in laboratory experiments presented here.

We have applied a relatively large amount of bulk strain in numerical models to show the nature of deformed shapes of inclusions in an interacting state. On the other hand, the solutions that are used for the numerical simulations have been obtained by imposing boundary conditions on spherical surfaces around the inclusion, which is valid only for small amounts of bulk strain. We make this departure intentionally to exaggerate the deformed geometry to show qualitatively the non-ideal shape of the inclusion.

In the two-dimensional consideration of numerical simulations we have used the ratio of inclusion diameter to inter-inclusion distance (a/b) as a parameter representing the effect of concentration. It is evident that the inter-inclusion distance (b) is related to the volume proportion of inclusions in the system. In the case of three-dimensional analysis, an equivalent parameter, $(a/b)^3$ can be considered as a measure of their volume concentration (Happel, 1957). However, the mathematical entity of this parameter is different from that of volume fraction, which is also a measure of volume concentration used in different analyses (e.g. Mandal et al., 2000; Treagus, 2002). The maximum value of $(a/b)^3$ can be one for systems with inclusions in contact with one another, whereas that of volume fraction cannot exceed 0.74.

6. Conclusions

The main conclusions of this analysis are outlined along the following points. (1) Spherical inclusions in multi-inclusion systems deform heterogeneously, and the principal parameters that control the deformation of the inclusions are: viscosity ratio of inclusion and matrix and concentration of inclusions. (2) For a given viscosity contrast, the ratio of flattening rate of stiff inclusions to that of the bulk system is larger for a larger concentration of inclusion. This factor needs to be considered for strain analysis of deformed rocks. (3) Circular sections of stiff inclusions are deformed into shapes resembling the geometry of super-ellipses, whereas those of soft inclusions develop geometry similar to sub-ellipses. (4) Stiff inclusions show increasing finite strain towards the center of inclusion. In contrast, soft inclusions describe a low-strain zone at the center. (5) Within inclusions, passive markers at right angles to bulk extension direction are distorted into curved shapes with the convex side facing outward in the case of stiff inclusion and inward in the case of soft inclusions.

Acknowledgements

We wish to thank two anonymous reviewers and Prof. C.W. Passchier for their comments that greatly contributed to the improvement of the paper. We also thank Professors S.H. Treagus, R.C. Fletcher and M. Bjornerud for giving many constructive comments on early versions of the manuscript. NM is grateful to DST, India for extending a financial support. SKS and GB wish to thank CSIR, India for providing research fellowships. CC acknowledges the infrastructural facilities provided by the Indian Statistical Institute, Calcutta.

Appendix A

Considering an irrotational type of bulk flow, the general expressions of the velocity fields inside and outside a spherical inclusion, after Lamb (1932), can be represented by:

$$u = \frac{1}{\eta}\sum\left\{\frac{r^2}{2(2n+1)}\frac{\partial p_n}{\partial x} + \frac{nr^{2n+3}}{(n+1)(2n+1)(2n+3)}\frac{\partial}{\partial x}\frac{p_n}{r^{2n+1}}\right\} + \sum\frac{\partial \Phi_n}{\partial x} \tag{A1a}$$

$$v = \frac{1}{\eta}\sum\left\{\frac{r^2}{2(2n+1)}\frac{\partial p_n}{\partial y} + \frac{nr^{2n+3}}{(n+1)(2n+1)(2n+3)}\frac{\partial}{\partial y}\frac{p_n}{r^{2n+1}}\right\} + \sum\frac{\partial \Phi_n}{\partial y} \tag{A1b}$$

$$w = \frac{1}{\eta}\sum\left\{\frac{r^2}{2(2n+1)}\frac{\partial p_n}{\partial z} + \frac{nr^{2n+3}}{(n+1)(2n+1)(2n+3)}\frac{\partial}{\partial z}\frac{p_n}{r^{2n+1}}\right\} + \sum\frac{\partial \Phi_n}{\partial z} \tag{A1c}$$

where p_n is a solid harmonic function of degree n for pressure distribution in the field. Φ_n is another solid harmonic function of degree n. η is the co-efficient of viscosity of the medium under consideration. For the present purpose the expressions of these two functions are considered retaining the harmonics of orders -3 and $+2$ (cf. Taylor, 1932; Happel, 1957; Gay, 1968a) for description

of the flow outside the inclusion. It then follows that:

$$\Phi_2 = \frac{1}{4}K\left(x^2 - y^2\right); \qquad \Phi_3 = B_{-3}\frac{\left(x^2 - y^2\right)}{r^5}; \qquad p_2\eta_m C_2 a^{-2}\left(x^2 - y^2\right); \qquad p_{-3}\eta_m A_{-3}a^3\frac{\left(x^2 - y^2\right)}{r^5} \tag{A2}$$

η_m is the co-efficient of viscosity of the matrix. Similarly, in order to describe the flow inside the inclusion the expressions of the functions can be chosen retaining harmonics of order 2 as:

$$\Phi_2' = B_2\left(x^2 - y^2\right); \qquad p_2' = \eta_i A_2 a^{-2}\left(x^2 - y^2\right) \tag{A3}$$

η_i is the co-efficient of viscosity of the inclusion. In Eqs. (A2) and (A3), K, B_{-3}, C_2, A_{-3}, B_2 and A_2 are constants, which need to be determined by applying boundary conditions.

Substituting the expressions of p_n and Φ_n in Eqs. (A1a)–(A1c), one can have the components of the flow perturbation outside the inclusion:

$$u^* = \frac{C_2}{21}\frac{r^2}{a^2}\left(5 - 2\frac{x^2 - y^2}{r^2}\right)x + \frac{1}{2}A_{-3}\frac{a^3}{r^3}\frac{x^2 - y^2}{r^2}x + B_{-3}\frac{a^5}{r^5}\left(2 - 5\frac{x^2 - y^2}{r^2}\right)x + \frac{1}{2}Kx \tag{A4a}$$

$$v^* = \frac{C_2}{21}\frac{r^2}{a^2}\left(-5 - 2\frac{x^2 - y^2}{r^2}\right)y + \frac{1}{2}A_{-3}\frac{a^3}{r^3}\frac{x^2 - y^2}{r^2}y + B_{-3}\frac{a^5}{r^5}\left(-2 - 5\frac{x^2 - y^2}{r^2}\right)y - \frac{1}{2}Ky \tag{A4b}$$

$$w^* = -\frac{2C_2}{21}\frac{r^2}{a^2}\left(\frac{x^2 - y^2}{r^2}\right)z + \frac{1}{2}A_{-3}\frac{a^3}{r^3}\frac{x^2 - y^2}{r^2}z - 5B_{-3}\frac{a^5}{r^5}\left(\frac{x^2 - y^2}{r^2}\right)z \tag{A4c}$$

The entire flow around the inclusion is then obtained by adding the perturbation to the homogeneous pure shear flow as:

$$u = u^* + \dot{\epsilon}x, v = v^* - \dot{\epsilon}y, w = w^* \tag{A5}$$

Similarly, substituting the expressions of ϕ_n' and p_n' in Eqs. (A1a)–(A1c), the velocity components of flow inside the inclusion follow:

$$u' = \frac{A_2}{21}\frac{r^2}{a^2}\left(5 - 2\frac{x^2 - y^2}{r^2}\right)x + 2B_2x \tag{A6a}$$

$$v' = \frac{A_2}{21}\frac{r^2}{a^2}\left(-5 - 2\frac{x^2 - y^2}{r^2}\right)y - 2B_2y \tag{A6b}$$

$$w' = -\frac{2A_2}{21}\frac{r^2}{a^2}\left(\frac{x^2 - y^2}{r^2}\right)z \tag{A6c}$$

In order to determine the constants, for convenience, the velocity functions in Eq. (A5) are transformed in terms of spherical coordinates (Fig. A1), as:

$$v_r^* = \left[\frac{1}{2}K + \frac{1}{7}C_2\frac{r^2}{a^2} + \frac{1}{2}A_{-3}\frac{a^3}{r^3} - 3B_{-3}\frac{a^5}{r^5}\right] r(\cos^2\theta - \sin^2\theta\cos^2\phi) \tag{A7a}$$

$$v_\theta^* = -\left[\frac{1}{2}K + \frac{5}{21}C_2\frac{r^2}{a^2} + 2B_{-3}\frac{a^5}{r^5}\right] r\sin\theta\cos\theta(1 + \cos^2\phi) \tag{A7b}$$

$$v_\phi^* = \left[\frac{1}{2}K + \frac{5}{21}C_2\frac{r^2}{a^2} + 2B_{-3}\frac{a^5}{r^5}\right] r\sin\phi\cos\phi\sin\theta \tag{A7c}$$

Similarly, after writing the velocity functions for flow inside the inclusion (Eqs. (A6a)–(A6c)) in terms of spherical coordinates, we have:

$$v_r' = \left[\frac{A_2}{7}\frac{r^2}{a^2} + 2B_2\right] r(\cos^2\theta - \sin^2\theta\cos^2\phi) \tag{A8a}$$

$$v_\theta' = -\left[\frac{5}{21}A_2\frac{r^2}{a^2} + 2B_2\right] r\sin\theta\cos\theta(1 + \cos^2\phi) \tag{A8b}$$

$$v_\phi' = \left[\frac{5}{21}A_2\frac{r^2}{a^2} + 2B_2\right] r\sin\phi\cos\phi\sin\theta \tag{A8c}$$

Eqs. (A7a)–(A7c) and (A8a)–(A8c) contain six unknown constants, which can be determined with the help of the following boundary conditions. As our model considers a non-slip condition at the matrix–inclusions interface, the conditions of continuity of the velocity and

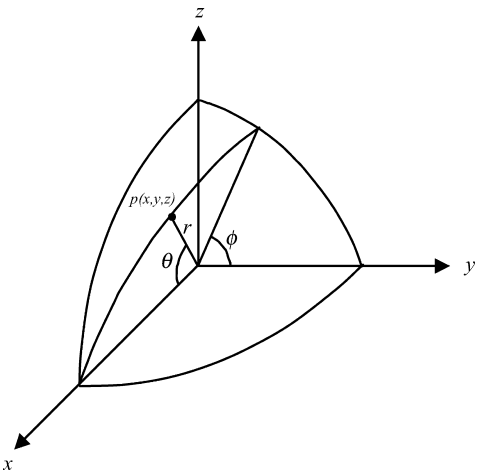

Fig. A1. Consideration of spherical co-ordinates with origin at the center of an inclusion.

stress fields across the interface ($r = a$) are imposed:

$$v_r = v'_r,\ v_\theta = v'_\theta,\ v_\phi = v'_\phi \tag{A9}$$

$$\sigma_{r\theta} = \sigma'_{r\theta},\ \sigma_{r\phi} = \sigma'_{r\phi},\ \sigma_{rr} = \sigma'_{rr} \tag{A10}$$

where

$$\sigma_{r\theta} = \eta_m\left[\frac{1}{r}\frac{\partial v_r}{\partial\theta} + \frac{\partial v_\theta}{\partial r} - \frac{v_\theta}{r}\right],$$

$$\sigma'_{r\theta} = \eta_i\left[\frac{1}{r}\frac{\partial v'_r}{\partial\theta} + \frac{\partial v'_\theta}{\partial r} - \frac{v'_\theta}{r}\right],$$

$$\sigma_{r\theta} = \eta_m\left[\frac{1}{r\sin\theta}\frac{\partial v_r}{\partial\phi} + \frac{\partial v_\phi}{\partial r} - \frac{v_\phi}{r}\right],$$

$$\sigma'_{r\phi} = \eta_i\left[\frac{1}{r\sin\theta}\frac{\partial v'_r}{\partial\phi} + \frac{\partial v'_\phi}{\partial r} - \frac{v'_\phi}{r}\right],$$

$$\sigma_{rr} = \left[-p + 2\eta_m\frac{\partial v_r}{\partial r}\right],$$

$$\sigma'_{rr} = \left[-p' + 2\eta_i\frac{\partial v'_r}{\partial r}\right]$$

After substituting the velocity components from Eqs. (A7a)–(A7c) and (A8a)–(A8c) in the above conditions (Eqs. (A9) and (A10)), the following equations are obtained:

$$\frac{A_2}{7} + 2B_2 = \dot{\epsilon} + \frac{1}{2}K + \frac{1}{7}C_2 + \frac{1}{3}A_{-3} - 3B_{-3} \tag{A11}$$

$$\frac{5}{21}A_2 + 2B_2 = \dot{\epsilon} + \frac{1}{2}K + \frac{5}{21}C_2 + 2B_{-3} \tag{A12}$$

$$\eta_m\left[-2\dot{\epsilon} - K - \frac{16}{21}C_2 - A_{-3} + 16B_{-3}\right] = \eta_i\left[-\frac{16}{21}A_2 - 4B_2\right] \tag{A13}$$

$$\eta_m\left[2\dot{\epsilon} + K - \frac{1}{7}C_2 - 3A_{-3} + 24B_{-3}\right] = \eta_i\left[-\frac{1}{7}A_2 + 4B_2\right] \tag{A14}$$

Now, in order to describe the interacting state of the inclusion in the system we follow Happel's (1957) model that considers a spherical envelope of radius b around the inclusion (b is the average inter-inclusion distance), and imposes the conditions of no normal flow and vanishing stress tensor components at the boundary of the envelope. It then follows that at $r = b$:

$$v^*_r = 0 \tag{A15}$$

$$\sigma^*_{r\theta} = \eta_m\left[\frac{1}{r}\frac{\partial v^*_r}{\partial\theta} + \frac{\partial v^*_\theta}{\partial r} - \frac{v^*_\theta}{r}\right]_{r=b} = 0 \tag{A16a}$$

$$\sigma^*_{r\phi} = \eta_m\left[\frac{1}{r\sin\theta}\frac{\partial v^*_r}{\partial\phi} + \frac{\partial v^*_\phi}{\partial r} - \frac{v^*_\phi}{r}\right]_{r=b} = 0 \tag{A16b}$$

From the above conditions, we have:

$$\frac{1}{2}K + \frac{1}{7}C_2\frac{b^2}{a^2} + \frac{1}{2}A_{-3}\frac{a^3}{b^3} - 3B_{-3}\frac{a^5}{b^5} = 0 \tag{A17}$$

$$K + \frac{16}{21}C_2\frac{b^2}{a^2} + A_{-3}\frac{a^3}{b^3} - 16B_{-3}\frac{a^5}{b^5} = 0 \tag{A18}$$

We now have six independent equations (Eqs. (A12)–(A14), (A17) and (A18)), relating the constants in the velocity functions. Following the conventional algebraic method, the solutions of the constants are:

$$A_{-3} = 2\dot{\epsilon}\frac{m-1}{LJ+I},$$

$$B_{-3} = \frac{2}{21}\dot{\epsilon}\frac{b^7}{a^7}\frac{m-1}{LJ+I}L,$$

$$C_2 = 2\dot{\epsilon}\frac{m-1}{LJ+I}L,$$

$$K = 2\dot{\epsilon}\frac{a^3}{b^3}\frac{m-1}{LJ+I},$$

$$A_2 = 2\dot{\epsilon}\left[\left(1 + \frac{5}{2}\frac{b^7}{a^7}\right)L - \frac{21}{4}\right]\frac{m-1}{LJ+I},$$

$$B_2 = \frac{1}{2}\dot{\epsilon}\left[1 + \left(\frac{m-1}{LJ+I}\right)\left(\frac{5}{2} - \frac{a^3}{b^3} - \frac{b^7}{a^7}L\right)\right] \tag{A19}$$

where

$$I = 1 + \frac{3}{2}m + (m-1)\frac{a^3}{b^3},$$

$$J = \left[\frac{16}{21}\left\{(1-m) - \frac{b^7}{a^7}(m+1)\right\} - \frac{1}{7}\frac{b^7}{a^7}m\right],$$

$$L = \frac{21\left(4 + \frac{19}{4}m\right)}{\left[19(m-1) + \frac{1}{2}\frac{b^7}{a^7}(80 + 95m)\right]}$$

m is the viscosity ratio of inclusion and matrix.

References

Bilby, B.A., Eshelby, J.D., Kundu, A.K., 1975. The change of shape of a viscous ellipsoidal region embedded in a slowly deforming matrix having different viscosity. Tectonophysics 28, 265–274.

Eshelby, J.D., 1957. The determination of the elastic field of an ellipsoidal inclusion, and related problems. Proceedings of the Royal Society of London A241, 376–396.

Freeman, B., 1987. The behaviour of deformable ellipsoidal particles in three-dimensional slow flows: implications for geological strain analysis. Tectonophysics 132, 297–309.

Gay, N.C., 1968a. Pure shear and simple shear deformation of inhomogeneous viscous fluids—I. Theory. Tectonophysics 5, 211–234.

Gay, N.C., 1968b. Pure shear and simple shear deformation of inhomogeneous viscous fluids—II. The determination of the total finite strain in a rock from objects such as deformed pebbles. Tectonophysics 5, 292–302.

Gay, N.C., Fripp, R.E.P., 1976. The control of ductility on the deformation of pebbles and conglomarates. Philosophical Transactions Royal Society 283, 109–128.

Happel, J., 1957. Viscosity of suspensions of uniform spheres. Journal of Applied Physics 28, 1288–1292.

Lamb, H., 1932. Hydrodynamics, Cambridge University Press, Cambridge.

Lisle, R.J., 1985. Geological Strain Analysis. A Manual for R_f/ϕ Technique, Pergamon Press, Oxford.

Lisle, R.J., 1988. The superellipsoidal form of coarse clastic sediment particles. Mathematical Geology 20, 879–890.

Lisle, R.J., Rondeel, H.E., Doorn, D., Brugge, J., Van de Gaag, P., 1983. Estimation of viscosity contrast and finite strain from deformed elliptical inclusions. Journal of Structural Geology 5, 603–609.

Mandal, N., Chakraborty, C., Samanta, S.K., 2000. An analysis of anisotropy of rocks containing shape fabrics of rigid inclusions. Journal of Structural Geology 22, 831–839.

Ramsay, J.G., 1967. Folding and Fracturing of Rocks, McGraw-Hill, New York.

Ramsay, J.G., Huber, M.I., 1983. The Techniques of Modern Structural Geology. Vol. 1. Strain Analysis, Academic Press, London.

Ramsay, J.G., Lisle, R., 2000. The Techniques of Modern Structural Geology. Vol. 3. Applications of Continuum Mechanics in Structural Geology, Academic Press, London.

Shimammoto, T., 1975. The finite element analysis of the deformation of a viscous spherical body embedded in a viscous medium. Journal of the Geological Society of Japan 81, 255–267.

Smith, R.B., 1975. A unified theory of the onset of folding, boudinage and mullion structures. Geological Society of America Bulletin 86, 1601–1609.

Taylor, G.I., 1932. The viscosity of a fluid containing small drops of another fluid. Proceedings of Royal Society London A 138, 41–48.

Treagus, S.H., 2002. Modelling the bulk viscosity of two-phase mixtures in terms of clast shape. Journal of Structural Geology 24, 57–76.

Treagus, S.H., Lan, L., 2000. Pure shear deformation of square objects and applications to geological strain analysis. Journal of Structural Geology 22, 105–122.

Treagus, S.H., Treagus, J.E., 2001. Effects of object ellipticity on strain, and implications for clast-matrix rocks. Journal of Structural Geology 23, 601–608.

Treagus, S.H., Hudleston, P.J., Lan, L., 1996. Non-ellipsoidal inclusions as geological strain markers and competence indicators. Journal of Structural Geology 18, 1167–1172.